Analytical Solution for Heat Transfer Problem in a Cross-Flow Plate Heat Exchanger

Mehdi Seddiq[a,*], Mehdi Maerefat[b]

[a]*Faculty of Engineering and Technology, Liverpool John Moores University, Liverpool, United Kingdom*
[b]*Department of Mechanical Engineering, Tarbiat Modares University, Tehran, Iran*

Abstract

Cross-flow plate heat exchangers are used for plenty of applications in industrial and domestic sectors, and the analysis of heat transfer is a key for the evaluation of their performance. There are challenges for an analytical study because heat transfer in each channel is governed by a partial differential equation coupled with temperature fields in the adjacent channels representing a three-dimensional problem. The problem is even more complicated in the turbulent regime as the effective thermal diffusivity varies within the channel cross-section. In the present study, a separate set of governing equations and boundary conditions are considered for each part of the heat exchanger. Appropriate profiles for the flow velocity and thermal diffusivity are substituted into the governing equations of the channels. The resulting partial differential equations in the channels are solved using the separation of variables method. There remains an unknown boundary condition linked to the temperature field on the plate surface which is considered to be in the form of a two-variable series function whose coefficients are calculated by applying energy balance between the two sides of the plate. The obtained solution provides explicit expressions for the temperature fields in the plate and channels. A scaling analysis is conducted showing that the model is valid when Peclet numbers in both hot and cold channels are not small. The results are compared with empirical data and a numerical model, and the accuracy of the derived

*Corresponding author
Email addresses: m.seddiq@ljmu.ac.uk (Mehdi Seddiq), maerefat@modares.ac.ir (Mehdi Maerefat)
URL: www.linkedin.com/in/mehdi-seddiq-8ab2a176 (Mehdi Seddiq), www.modares.ac.ir/~maerefat (Mehdi Maerefat)

August 23, 2020

heat transfer coefficients is investigated. In harmony with the scaling analysis, a close agreement is observed in both laminar and turbulent flows for moderate and high Prandtl numbers and when Peclet number is greater than 1000 in the case of turbulent flow.

Keywords: Plate Heat Exchanger, Heat transfer, Analytical Solution, Coupled Partial Differential Equations.

Nomenclature

Latin symbols

C	heat capacity rate of flow, Eq.57, W/K
Cp	specific thermal capacity, J/(kgK)
D	hydraulic diameter of channel, m
f_u	velocity profile form function Eq. 2
f_ϵ	eddy diffusivity profile form function Eq. 3
h	convective heat transfer coefficient, W/m^{2}K
H_h& H_c	height of hot & cold channels, m
H_P	thickness of plate, m
k	thermal conductivity, W/(mK)
L& W	length of hot & cold channels, m
L_0& W_0	Stabilized lengths of hot & cold channels, m
Nu	Nusselt number, dimensionless
Pe	Peclet number, $Pe = Re\,Pr$, dimensionless
Pr	Prandtl number, Eq. 1d, dimensionless
Pr_t	turbulent Prandtl number, dimensionless

Q	amount of heat transfer, W
q_p	local heat flux through plate, $\mathrm{W/m^2}$
q_p^*	local heat flux through plate, dimensionless
Re	Reynolds number, Eq. 1d, dimensionless
T	Temperature, K
t	time, s
U	overal heat transfer coefficient, $\mathrm{W/m^2K}$
u	velocity, m/s
X	x-dependent part of solution for hot channel
x, y, z	coordinations, dimensionless
x_d, y_d, z_d	coordinations, m
Y	y-dependent part of solution for cold channel
Z	z-dependent part of solution for channels

Greek symbols

α	thermal diffusivity, $\mathrm{m^2/s}$
ϵ_H	thermal eddy diffusivity, $\mathrm{m^2/s}$
ϵ_M	momentum eddy diffusivity, $\mathrm{m^2/s}$
λ	eigenvalue
Φ	plate surface temperature, dimensionless
ρ	density, $\mathrm{kg/m^3}$
ρ_m, ρ_n	eigenvalue-dependent parameters, Eq.s 28 & 37
σ	weight function, Eq. 25 & 38
θ	temperature, dimensionless

ξ rejected solution for Z, Eq. A.1

ζ accepted solution for Z, Eq.s A.1 & 23

Subscripts

c cold channel

h hot channel

hom solution of homogeneous equation

m eigenvalue index

p plate

Abbreviations

MEE Membrane Enthalpy Exchanger

PHE Plate Heat Exchanger

1. Introduction

A plate heat exchanger (PHE) or more accurately, flat plate heat exchanger consists of multiple channels separated by flat plates allowing fluids with different temperatures to exchange heat without mixing. It has numerous applications in different fields. In air conditioning, PHEs are used as air-to-air heat recovery ventilators to reduce the energy consumed for treating fresh supply air. Detailed information about different types and arrangements, design methods and construction could be found in [1, p. 347-372]. In some applications, a similar device named as membrane enthalpy exchanger (MEE) is used where a membrane replaces the plate to allow a selective mass transfer as well as the heat exchange.

A variety of different surface types are used for the plate. Corrugated-surface plates are shaped into parallel rows of ridges and grooves and are popular for their enhanced heat transfer coefficients. Flat-surface types have plates without waves or other irregularities in their surface in a macroscopic scale, and they are used in some applications due to advantages such as reduced fouling problem and reduced need for cleaning, ease of maintenance and lower pressure drops [1].

The analysis of heat transfer in PHEs and MEEs have been the subject of many researches most of which have employed a numerical scheme to solve the system of governing equations.

Gut and Pinto [2] developed a one-dimensional model for a PHE package containing multiple channels and obtained a set of ordinary differential equations. They proposed an algorithm including a numerical method to calculate the pressure and temperature for different configurations. Saman and Alizadeh [3] studied heat and humidity transfer through the membrane in an MEE both by a numerical model and an experimental set-up. Zhang [4] used a numerical method to model the 3-dimensional heat and mass transfer problem in a cross-flow MEE. Huang et al. [5] modelled heat and mass transfer in the laminar flow of an MEE for air dehumidification applications by a numerical method. In both [4] and [5], the influence of mass transfer on the governing equations for energy balance has been neglected. Simonetti et al. [6] conducted a numerical study on counter-flow PHEs followed by an experimental test, and analysed the effect of different flow mixing devices. Vali et al. [7] provided a simplified 2-D model for the problem of heat and mass transfer in a cross-flow MEE and developed a numerical code for the model. Jun and Puri [8] developed a 2-D numerical model to study fouling performance in a PHE with flat-surface plates.

In some studies, commercial numerical software has been employed for the numerical study. As instances, Galeazzo et al. [9] studied PHEs with flat surface numerically and also in experimental tests. Deshko et al. [10] developed a numerical model and also used a commercial modelling package to study heat and mass transfer in a cross-flow air-to-air MEE. Dvorák and Vit [11] considered a counter-flow PHE to be consist of cross-flow parts with flat-surface plates and counter-flow parts with undulated plate, and used a commercial package to model heat transfer.

Analytical solutions provide expressions for temperature distribution, heat flux and performance in terms of parameters rather than specific values for them and hence, they can offer valuable understandings about the effect of different conditions on the desired parameters. In the following, a few works with analytical approaches are reviewed.

Zaleski and Klepacka [12] represented an analytical method to calculate temperatures in parallel-flow PHEs with multiple channels. Srihari et al. [13] developed a time-dependent one-dimensional model for PHE in the form of a set of PDEs. They then solved the equations partly analytically by Laplace transform and partly by a numerical scheme. Zhang and Niu [14] conducted a 2-D analysis on heat and mass transfer in an MEE and provided simplified expressions to esti-

mate the sensible and latent effectiveness. Khaled [15] analysed the 2-D problem of heat transfer in a special design of a counter-flow PHE in which the cold and hot sides are separated by an auxiliary fluid channel aiming to enhance the rate of heat exchange. He developed a numerical model to solve the resulting PDEs and derived an approximate analytical solution for a simplified case. Yeh and Ho [16] conducted an analytical study for 1-D heat transfer in a parallel-flow heat exchanger similar to a plate type in which one channel is divided into two sub-channels resulting in cocurrent and countercurrent flows. Lu et al. [17] derived 1-D analytical solutions for the velocity and temperature in a parallel-flow PHE which is partially filled with metal foams. Sangsawang et al. [18] analysed heat transfer in a cross-flow PHE with triangular channels and developed a model in which the conduction heat transfer within the fluids in the channels was neglected and the temperature at each section of the channels was considered to be uniform.

The nature of heat transfer in PHEs of cross-flow type is three-dimensional which makes it a more complex problem and there is a shortage of analytical works for this type of heat exchangers. In the present study, we have derived an explicit solution for the temperature distribution by considering separate heat transfer equations for the plate and channels, solving the problem for each part and reconnecting the equations for neighbouring parts in the form of boundary conditions.

2. Mathematical Model

A schematic diagram with the coordination system for a multiple-channel cross-flow flat PHE is displayed in Fig. 1. Note that a specific z-axis is defined for each part.

The mathematical model has been developed for a flat PHE with the following specifications. The PHE consists of several consecutive hot and cold channels separated by rectangular plates through which the heat exchange between the channels at the two sides is carried out. The flows in the channels are single-phase, incompressible and steady. There is no secondary flow or flow leakage. The fluids at the entrances are in uniform temperatures throughout the cross-section. In each channel and the plate, the changes in the properties due to temperature variation are negligible. However, the fluid in each side can be different from the other one. Furthermore, we use the properties and assumptions in the mathematical model as fallows:

1. The plate has a flat surface, but it can be smooth or rough.

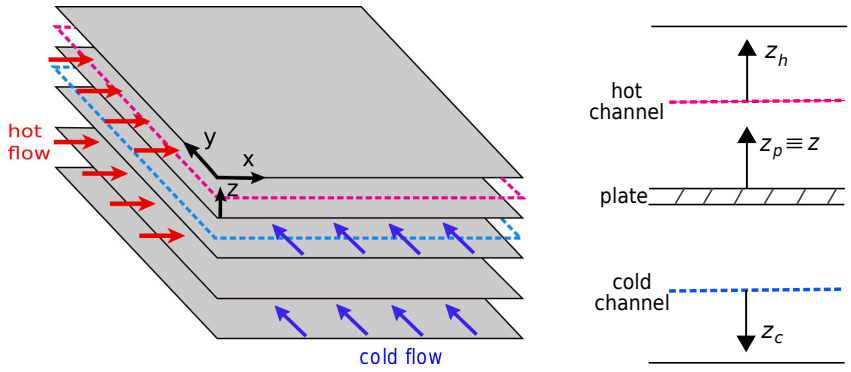

Figure 1: A schematic for the channels in a PHE and the coordination system used for the analysis. The dashed lines represent the planes of symmetry in the middle of the channels. Note that the origins of z_h and z_c are at the middle of the channels, and the origin of z_p is at the hot side of the plate surface

2. Hydrodynamic entrance effects are negligible and hence, the flows are considered to be hydrodynamically fully developed.

3. The length and width are sufficiently large so that the effect of the boundary conditions of the side walls (the peripheral walls of channels) on the overall heat transfer is negligible both in the channels and the plate.

4. Transversal heat conduction, i.e. conduction in x or y direction is negligible.

Assumption 1 refers to the flat-surface type of PHEs as explained earlier. Assumption 2 represents a condition which is more general than the usual restrictions as the results in the literature are usually limited to fully developed conditions. We will scrutinise the rest of the assumptions in the subsequent sections, where the results from the present model are compared with the empirical results. We will also conduct a scaling analysis to investigate assumption 4, which will provide a theoretical criterion for the limits imposed by the assumption.

We introduce dimensionless forms of the parameters as below,

$$x = \frac{x_d}{L}, \qquad y = \frac{y_d}{W}, \tag{1a}$$

$$z \equiv z_h = \frac{z_{h,d}}{H_h/2} \text{ (Hot side)}, \quad z \equiv z_p = \frac{z_{p,d}}{H_p} \text{ (Plate)}, \quad z \equiv z_c = \frac{z_{c,d}}{H_c/2} \text{ (Cold side)}, \tag{1b}$$

$$\theta = \frac{T - T_c^0}{T_h^0 - T_c^0}, \tag{1c}$$

$$Re = \frac{\overline{u}D}{\nu}, \quad Pr = \frac{\alpha}{\nu}. \tag{1d}$$

The symbols are introduced in the nomenclature. Note that x, y and z are the coordination axes as introduced in Fig. 1 and are dimensionless unless specified by a d index. The hydraulic diameter D is calculated based on the geometry of a channel consisting of two wide parallel plates which for the hot side is $D_h = 2H_h$. The indexes h, c and p indicate the hot channel, cold channel and plate respectively. However, wherever none of those indexes are shown, the hot channel is intended.

Velocity profile

By considering the flow in the channels to be hydraulically fully developed, the velocity varies only in the z- direction and one can write,

$$u_h(z_h) = \overline{u_h}\, f_u(z_h), \tag{2a}$$

where f_u is the profile form function for the velocity in the half-channel and depends on the flow regime as the following,
Laminar flow (parabolic variations),

$$f_u(z) = (1 - z^2), \tag{2b}$$

Turbulent flow (power law),

$$f_u(z) = (z + 1)^{1/n}, \tag{2c}$$

where the parameter n varies slightly with the Reynolds number, e.g. $n \approx 6$ for $Re < 10^4$ and $n \approx 7$ for $Re = 10^5$ [19, p. 423-424]. The power-law model, overestimates the values of the velocity near the boundary and a linear profile

according to the laminar sublayer model gives more accurate values [19, p. 422-423]. We can use a single profile for the whole cross-section by combining the linear and power-law profiles, i.e.

$$f_u(z) = (1 - e^{c_{lin}z}) f_{u,lin}(z) + e^{c_{pow}z} f_{u,pow}(z), \tag{2d}$$

where $f_{u,lin}$ is the linear velocity profile as mentioned above for to the laminar sublayer and $f_{u,pow}$ is the power-law velocity profile as in Eq.2c for the rest of the channel. c_{lin} and c_{pow} are positive constants and are determined in a way that the combined profile provides reasonable agreements with the sublayer and power-law models separately. The coefficient for the linear part (the first term on the right-hand side) varies from nearly 1 at the wall ($z = -1$) to 0 at the channel centre ($z = 0$), and the coefficient for the power-law profile (the second term) varies in the opposite way.

Thermal eddy diffusivity

The eddy diffusivity ϵ_H does not appear in laminar flows, i.e.

$$\epsilon_H(z_h) = 0. \tag{3a}$$

In the turbulent regime, the thermal eddy diffusivity is related to the momentum eddy diffusivity through the turbulent Prandtl number $Pr_t = \frac{\epsilon_M}{\epsilon_H}$ which is thought to be constant with the order of magnitude of unity [20, p. 239] & [21, p. 45]. We define a profile form function $f_\epsilon(z)$ to describe the variations of the momentum eddy diffusivity within the channel. Depending on the distance from the wall, different curves have been suggested in the literature. Ref. [22] represents unified expressions for the whole channel based on which, we approximate the thermal eddy diffusivity across the rectangular channels of the present study according to the coordination shown in Fig. 1 as below,

$$\epsilon_H(z_h) = \epsilon_0 Pr_t f_\epsilon(z_h), \tag{3b}$$

$$f_\epsilon(z) = (1 - z^4). \tag{3c}$$

where $\epsilon_0 = \frac{1}{8} D\, u_* \kappa$ in which D is the hydraulic diameter of the channel, u_* is the shear velocity and can be calculated based on the channel maximum velocity [23, p. 602] and $\kappa = 0.41$ is the von Karman constant.

A similar set of equations can be written for the cold side.

Governing equations

Regarding the conservation of energy for the turbulent flow in an incompressible medium without thermal source and viscous dissipation [20, p. 327], the dimensionless form of the equation for a hot channel of a flat PHE can be written as

$$\frac{1}{L^2}\frac{\partial}{\partial x}\left((\alpha+\epsilon_H)\frac{\partial\theta}{\partial x}\right)+\frac{1}{W^2}\frac{\partial}{\partial y}\left((\alpha+\epsilon_H)\frac{\partial\theta}{\partial y}\right)+\frac{1}{(H_h/2)^2}\frac{\partial}{\partial z_h}\left((\alpha+\epsilon_H)\frac{\partial\theta}{\partial z_h}\right)-u_h\frac{1}{L}\frac{\partial\theta}{\partial x}=0. \tag{4}$$

We note that the velocity u in the hot and cold channels is purely in x and y directions respectively.

Assumption 4 leads the conduction in x and y directions to be negligible. By further arrangements using Eq.s 2a and 1d, we can derive a full dimensionless form of the governing equations for the channels as below,

hot channel:

$$\frac{8L}{H_h}\frac{\partial}{\partial z_h}\left((1+\frac{\epsilon_H}{\alpha})\frac{\partial\theta}{\partial z_h}\right)-Pe\,f_u(z_h)\frac{\partial\theta}{\partial x}=0, \tag{5}$$

cold channel:

$$\frac{8W}{H_c}\frac{\partial}{\partial z_c}\left((1+\frac{\epsilon_{H,c}}{\alpha_c})\frac{\partial\theta}{\partial z_c}\right)-Pe_c\,f_u(z_c)\frac{\partial\theta}{\partial y}=0. \tag{6}$$

In the plate, there is pure conduction, thus,

$$\frac{1}{L^2}\frac{\partial^2\theta}{\partial x^2}+\frac{1}{W^2}\frac{\partial^2\theta}{\partial y^2}+\frac{1}{H_p^2}\frac{\partial^2\theta}{\partial z_p^2}=0. \tag{7}$$

By neglecting the transversal heat conductions, the following ordinary differential equation is obtained,

$$\frac{d^2\theta}{dz_p^2}=0 \tag{8}$$

Boundary conditions

As a commonly used condition in heat exchangers, the temperature of fluids at the entrances are considered to be uniform, therfore,

$$\theta(x=0,y,z_h)=1, \tag{9a}$$
$$\theta(x,y=0,z_c)=0. \tag{9b}$$

Since a typical PHE consists of several similar pairs of hot and cold channels, the conditions of flow inside a hot/ cold channel will be similar to its neighbouring hot/ cold channel provided that the channel is not close to an ending side of the heat exchanger. Thus, symmetry conditions hold at the middle of each channel giving rise to zero temperature gradients on the z-direction,

$$\frac{\partial \theta}{\partial z_h}|_{z_h=0} = 0, \tag{9c}$$

$$\frac{\partial \theta}{\partial z_c}|_{z_c=0} = 0. \tag{9d}$$

Because the transversal heat conductions are neglected (assumption 4) and the corresponding conduction terms do not appear in the governing equations, the model does not contain any boundary condition for the sides, i.e. y-direction in the hot and x-direction in the cold channels.

Decoupling the problem and deriving additional boundary conditions

To obtain a solution for the system of differential equations in the heat exchanger, we divide the domain into three regions, hot flow, plate and cold flow each with a separate differential equation and boundary conditions. The regions are linked through boundary conditions at the interfaces between the channels and plate. If assumption 1 holds, by considering temperature continuity at the plate interface with the fluid, we have

$$\theta(x, y, z_h = -1) = \theta(x, y, z_p = 0), \tag{10a}$$

$$\theta(x, y, z_c = -1) = \theta(x, y, z_p = -1). \tag{10b}$$

Consequently, by considering two unknown functions $\Phi(x, y)$ and $\Phi_c(x, y)$ as the temperature field of the plate surfaces at the hot and cold sides respectively, two separate equations are derived from each of the above equations. Eq. 10a provides the following boundary conditions,

$$\theta(x, y, z_h = -1) = \Phi(x, y), \tag{11a}$$

$$\theta(x, y, z_p = 0) = \Phi(x, y), \tag{11b}$$

and Eq. 10b leads to

$$\theta(x, y, z_p = -1) = \Phi_c(x, y), \tag{11c}$$
$$\theta(x, y, z_c = -1) = \Phi_c(x, y). \tag{11d}$$

The unknown boundary values $\Phi(x, y)$ and $\Phi_c(x, y)$ will be calculated later as a part of the solution.

3. Solving the governing differential equations

The problem of heat transfer in the hot side consists of the partial differential equation (PDE) 5 with the boundary condition Eq.s 9a, 9c and 11a. Similarly, for the cold side, the set of equations is 6, 9b, 9d and 11d. Although the governing equations are reduced to 2-D, since the boundary conditions are functions of both x and y, the temperature distribution will be 3-D.

Solution for the plate

The problem in the plate is an ordinary differential equation 8 with Eq.s 11b and 11c as the boundary conditions which is immediately solved:

$$\theta(x, y, z_p) = (\Phi(x, y) - \Phi_c(x, y))\, z_p + \Phi(x, y). \tag{12}$$

which explicitly includes the dimensionless heat flux through the plate,

$$q_p^* = \Phi(x, y) - \Phi_c(x, y). \tag{13}$$

Solution for the hot channel

The PDE of each channel defines an initial boundary value problem which is solved by the separation of variables method [24]. Regarding the hot channel, the solution of Eq. 5 is assumed to be

$$\theta(x, y, z_h) = \theta_{hom}(x, y, z_h) + \Phi(x, y), \tag{14}$$

which defines a new problem for θ_{hom} with the below homogeneous boundary condition instead of Eq. 11a

$$\theta_{hom}(x, y, z_h = -1) = 0, \tag{15}$$

The PDE in the new problem is inhomogeneous,

$$\frac{1}{Pe\, f_u(z_h)} \frac{8L}{H_h} \frac{\partial}{\partial z_h} \left((1 + \frac{\epsilon_H}{\alpha}) \frac{\partial \theta_{hom}}{\partial z_h} \right) - \frac{\partial \theta_{hom}}{\partial x} = \Phi_x, \tag{16}$$

where $\Phi_x = \Phi_x(x, y) = \frac{\partial}{\partial x}\Phi(x, y)$. The other boundary conditions are

$$\theta_{hom}(x = 0, y, z_h) = \theta_h - \Phi(0, y), \tag{17}$$

$$\frac{\partial \theta_{hom}}{\partial z_h}|_{z_h=0} = 0. \tag{18}$$

The homogeneous form of Eq. 16 i.e. the equation without the term Φ_x is assumed to have a solution in the form,

$$\theta_{hom}(x, y, z_h) = X(x, y)Z(z_h), \tag{19}$$

which leads to two ordinary differential equations as below,

$$\frac{1}{Pe\, f_u(z_h)} \frac{8L}{H_h} \frac{1}{Z} \frac{\partial}{\partial z_h} \left((1 + \frac{\epsilon_H}{\alpha}) \frac{\partial Z}{\partial z_h} \right) = -\lambda, \tag{20}$$

$$\frac{1}{X} \frac{\partial X}{\partial x} = -\lambda, \tag{21}$$

where λ is a constant known as the eigenvalue which is positive because it can be shown that otherwise, the boundary condition equations would result in the trivial solution $Z(z_h) = 0$.

Eq. 20 is solved using series solution method which leads to an infinite power series for $Z(z_h)$ consisting of two orthogonal solutions $\zeta(z_h)$ and $\xi(z_h)$, and the general solution is in the form $Z(z_h) = C_1\zeta(z_h) + C_2\xi(z_h)$. More details about the solution procedure are given in Appendix A. Eq. 18 gives a boundary condition as $Z'(0) = 0$ which leads to $C_2 = 0$ and the solution is reduced to $Z(z_h) = C_1\zeta(z_h)$.

The other boundary condition comes from Eq. 15 which is used to calculate eigenvalues

$$\zeta(z_h = -1) = 0. \tag{22}$$

The above equation gives an infinite number of answers for λ. From now on, λ_m indicates the m-th answer related to the m-th eigenfunction $\zeta_m(z_h)$, and a smaller m denotes a smaller λ_m. Hence, the functional form of the solution for $Z(z_h)$ is

$$Z(z_h) = \zeta_m(z_h). \tag{23}$$

Eq. 20 defines a Sturm-Liouville Eigenvalue problem in the form

$$\frac{\partial}{\partial z_h}\left((1+\frac{\epsilon_H}{\alpha})\frac{\partial Z}{\partial z_h}\right)+\frac{H_h}{8L}Pe\, f_u(z_h)\lambda_m Z=0, \tag{24}$$

whose the weight function is

$$\sigma(z_h)=\frac{H_h}{8L}Pe\, f_u(z_h). \tag{25}$$

Any piecewise smooth function in the problem can be expanded in terms of the eigenfunctions $\zeta_m(z_h)$. Accordingly, $\Phi_x(x,y)$ can be expressed as

$$\Phi_x(x,y)=\sum_{m=1}^{\infty}\zeta_m(z_h)\Phi_{x,m}(x,y), \tag{26}$$

where we have

$$\begin{aligned}\Phi_{x,m}(x,y) &= \frac{\int_0^1 \Phi_x(x,y)\zeta_m(z_h)\sigma(z_h)dz_h}{\int_0^1 \zeta_m^2(z_h)\sigma(z_h)dz_h}\\ &= \rho_m\Phi_x(x,y),\end{aligned} \tag{27}$$

where the constants ρ_m are formulated by

$$\rho_m=\frac{\int_0^1 \zeta_m(z_h)\sigma(z_h)dz_h}{\int_0^1 \zeta_m^2(z_h)\sigma(z_h)dz_h}. \tag{28}$$

Also, the expression in Eq. 19 for θ_{hom} can be written as

$$\theta_{hom}(x,y,z_h)=\sum_{m=1}^{\infty}X_m(x,y)\zeta_m(z_h). \tag{29}$$

The functional form of the solution for homogeneous problem is identical to the inhomogeneous one. Thus, substituting the expression in Eq. 29 for θ_{hom} alongside the expression in Eq. 26 for $\Phi_x(x,y)$ into Eq. 16, one can write

$$\sum_{m=1}^{\infty}\left[\frac{1}{Pe\, f_u(z_h)}\frac{8L}{H_h}\frac{\partial}{\partial z_h}\left((1+\frac{\epsilon_H}{\alpha})\frac{\partial\zeta_m}{\partial z_h}\right)X_m-\zeta_m\frac{\partial X_m}{\partial x}\right]=\sum_{m=1}^{\infty}\zeta_m\Phi_{x,m}. \tag{30}$$

According to Eq.s 23 and 24, the first term in the above equation is equal to $-\lambda_m \zeta_m X_m$, therefore, the terms of the series in the equation reduce to

$$\lambda_m X_m(x,y) + \frac{\partial X_m(x,y)}{\partial x} = -\Phi_{x,m}(x,y). \tag{31}$$

The solution of the above ordinary differential equation is

$$X_m(x,y) = \left(\int_0^x -\Phi_{x,m}(x,y) e^{\lambda_m x} dx + c_{h,m}(y) \right) e^{-\lambda_m x}, \tag{32}$$

where $c_{h,m}(y)$ is the parameter of the solution for the differential equation.

Now, by referring to Eq. 14, the solution of the problem for the hot channel ($0 \leqslant z_h \leqslant 1$) will be in the following form

$$\theta(x,y,z_h) = \sum_{m=1}^{\infty} \left[\left(\int_0^x -\Phi_{x,m}(x,y) e^{\lambda_m x} dx + c_{h,m}(y) \right) e^{-\lambda_m x} \zeta_m(z_h) \right] + \Phi(x,y) \tag{33}$$

By applying the boundary condition Eq. 9a we have

$$(1 - \Phi(0,y)) = \sum_{m=1}^{\infty} [c_{h,m}(y) \zeta_m(z_h)].$$

Multiplying both sides of the above equation by $\zeta_{m'}(z_h)\sigma(z_h)$ and then integrating, we can write

$$\int_0^1 (1 - \Phi(0,y)) \, \zeta_{m'}(z_h)\sigma(z_h) dz_h = \int_0^1 \sum_{m=1}^{\infty} [c_{h,m}(y) \zeta_m(z_h) \zeta_{m'}(z_h) \sigma(z_h)] dz_h.$$

Due to the orthogonality of the Sturm-Liouville eigenfunctions ζ_m and $\zeta_{m'}$, the right-hand side of the above equation is zero except for the case $m = m'$. m' on the left-hand side is a free index and can be replaced by m. Therefore,

$$\int_0^1 (1 - \Phi(0,y)) \, \zeta_m(z_h)\sigma(z_h) dz_h = c_{h,m}(y) \int_0^1 \zeta_m^2(z_h)\sigma(z_h) dz_h.$$

which yields an expression for c_h as

$$c_{h,m}(y) = \rho_m \left(1 - \Phi(0,y)\right). \tag{34}$$

Thus,

$$\theta(x,y,z_h) = \sum_{m=1}^{\infty}\left[\left(\int_0^x -\Phi_x(x,y)e^{\lambda_m x}dx + (1-\Phi(0,y))\right)\rho_m e^{-\lambda_m x}\zeta_m(z_h)\right] + \Phi(x,y). \tag{35}$$

To complete the solution, we need to obtain the function $\Phi(x,y)$. For this aim, it is necessary to solve the PDE in the cold channel and associate the answer to the above solution for the hot channel.

Solution for the cold channel

The solution of Eq.s 6, 9b, 9d, and 11d for the cold channel is similar to that of the hot side, i.e.

$$\theta(x,y,z_c) = \sum_{n=1}^{\infty}\left[\left(\int_0^y -\Phi_{c,y}(x,y)e^{\lambda_n y}dy - \Phi_c(x,0)\right)\rho_{c,n}e^{-\lambda_n y}\zeta_{c,n}(z_c)\right] + \Phi_c(x,y), \tag{36}$$

$$\rho_{c,n} = \frac{\int_0^1 \zeta_{c,n}(z_c)\sigma_c(z_c)dz_c}{\int_0^1 \zeta_{c,n}^2(z_c)\sigma_c(z_c)dz_c}, \tag{37}$$

$$\sigma_c(z_c) = \frac{H_c}{8W}Pe_c\, f_u(z_c). \tag{38}$$

where the subscript c indicates the cold channel in analogy to the hot side and $\Phi_{c,y}$ is the y-derivative. Similar to the hot side, $\zeta_{c,n}(z_c)$ is a solution for the ordinary differential equation of the Z part (written below) which can satisfy the boundary condition 9d.

$$\frac{1}{Pe_c\, f_{u,c}(z_c)}\frac{8W}{H_c}\frac{1}{Z_c}\frac{\partial}{\partial z_c}\left((1+\frac{\epsilon_{Hc}}{\alpha_c})\frac{\partial Z_c}{\partial z_c}\right) = -\lambda_{c,n}. \tag{39}$$

The eigenvalues $\lambda_{c,n}$ are found from the following equation

$$\zeta_c(z_c = -1) = 0. \tag{40}$$

Combining the solutions

With assumption 1, by taking into account the continuity of heat flux at the plate interface with the fluid, two additional equations are obtained, i.e.

$$\frac{k_h}{H_h/2}\frac{\partial\theta}{\partial z_h}|_{z_h=-1} = \frac{k_p}{H_p}\frac{\partial\theta}{\partial z_p}|_{z_p=0}, \tag{41}$$

$$\frac{k_c}{H_c/2}\frac{\partial\theta}{\partial z_c}|_{z_c=-1} = -\frac{k_p}{H_p}\frac{\partial\theta}{\partial z_p}|_{z_p=-1}, \tag{42}$$

where k_h and k_c and are the thermal conductivities of the fluids in the hot and cold channels respectively, and k_p is the plate thermal conductivity. The negative sign in Eq. 42 is because the directions of z coordinates in the cold channel and plate are opposite.

Substituting into the above equations from the expressions obtained for temperature, Eq.s 35, 12 and 36, one can write

$$\sum_{m=1}^{\infty}\left[\left(\int_0^x -\Phi_x(x,y)e^{\lambda_m x}dx + (1-\Phi(0,y))\right)\rho_m e^{-\lambda_m x}\acute{\zeta_m}(-1)\right] = \Phi(x,y) - \Phi_c(x,y), \tag{43}$$

$$\sum_{n=1}^{\infty}\left[\left(\int_0^y -\Phi_{c,y}(x,y)e^{\lambda_n y}dy - \Phi_c(x,0)\right)\rho_{c,n}e^{-\lambda_n y}\acute{\zeta_{c,n}}(-1)\right] = -\left(\Phi(x,y) - \Phi_c(x,y)\right), \tag{44}$$

where

$$\acute{\zeta_m}(-1) = \frac{k_h}{k_p}\frac{H_p}{H_h/2}\frac{\partial\zeta_m(z_h)}{\partial z_h}|_{z_h=-1}, \tag{45a}$$

$$\acute{\zeta_{c,n}}(-1) = \frac{k_c}{k_p}\frac{H_p}{H_c/2}\frac{\partial\zeta_{c,n}(z_c)}{\partial z_c}|_{z_c=-1}. \tag{45b}$$

Eq. 43 offers an expression for $\Phi_c(x,y)$, i.e.

$$\Phi_c(x,y) = \Phi(x,y) - \sum_{m=1}^{\infty}\left[\left(\int_0^x -\Phi_x(x,y)e^{\lambda_m x}dx + (1-\Phi(0,y))\right)\rho_m e^{-\lambda_m x}\acute{\zeta_m}(-1)\right]. \tag{46}$$

In Eq. 44, $\Phi_c(x,y)$ is replaced by the above expression resulting in an equation with only one unknown function $\Phi(x,y)$. $\Phi(x,y)$ is then found by considering an ansatz of two-variable power series. The details of the procedure are provided in Appendix B.

4. Analysis of the solution

The present solution gives the temperature at any point within the channels and the plate. It can also be used to derive expressions for the heat flux at a desired location and convection coefficient on each surface. The mathematical formulations are expressed as infinite series with oscillating terms related to the

eigenvalues λ_m. As more terms are included, more accurate values are obtained. The terms with $\lambda_m > 10$ have smaller shares in the answer and they require dealing with large numbers, and hence, they can be neglected. However, for an acceptable accuracy, it is necessary that the largest eigenvalue is sufficiently large. Here, we have rejected the results with largest λs less than 1.

The smallest eigenvalue, λ_1 is in particular important as it has the greatest contribution in the rate of temperature change along the flow direction. By Substituting the first terms of ζ into Eq. 22, one can obtain an estimation for λ_1 which indicates that it is almost proportional to the inverse of the d parameters (see Appendix A), i.e.

$$\lambda_1 \propto \frac{L}{H_h}\frac{(1+\epsilon_0/\alpha)}{Pe} \tag{47}$$

4.1. A validity limit for the solution

It is expected that transversal heat conductions impose the major restrictions on the present model for a typical flat PHE. Therefore, we conduct a scaling analysis to investigate the conditions under which assumption 4 holds.

We first regard the hot channel. Assumption 4 indicates that z-conduction in the channel must be balanced almost entirely by the heat convection. Thus, regarding Eq. 4 we need to have

$$O\left(\frac{1}{(H_h/2)^2}\frac{\partial}{\partial z_h}\left((\alpha+\epsilon_H)\frac{\partial\theta}{\partial z_h}\right)\right) \approx O\left(u_h\frac{1}{L}\frac{\partial\theta}{\partial x}\right). \tag{48}$$

The driving force for temperature variations within the plate in x and y directions, i.e. $\Delta\theta_x$ and $\Delta\theta_y$, comes from the difference between the local values of the temperature across the plate thickness, i.e. $\Delta\theta_{H_p}$. Thus, $\Delta\theta_x \lesssim \Delta\theta_{H_p}$ and $\Delta\theta_y \lesssim \Delta\theta_{H_p}$. In a cross-flow heat exchanger, $\Delta\theta_{H_p}$ is decreased as the distance from an entrance becomes more. In sufficiently large distances from the entrance, i.e. L_0, the temperature is stabilized and does not varies noticeably by further distance from the entrance. The temperature variation from the entrance to L_0 is in the same order as the maximum temperature variation across the channel. Therefore, by considering a section of the channel with the length L_0, we can find an estimation for L_0,

$$L_0 \approx \frac{1}{4}H_h\frac{u_h H_h}{(\alpha+\epsilon_H)}. \tag{49}$$

The assumption also implies that the x-conduction term is negligible compared

to the convection term,

$$u_h \frac{1}{L_0}\frac{\partial \theta}{\partial x} \gg \frac{1}{L_0^2}\frac{\partial}{\partial x}\left((\alpha + \epsilon_H)\frac{\partial \theta}{\partial x}\right),$$

or

$$\frac{u_h L_0}{(\alpha + \epsilon_H)} \gg 1.$$

By substituting for L_0 in the above equation from Eq. 49 we obtain

$$\frac{u_h 2H_h}{(\alpha + \epsilon_H)} \gg 1, \tag{50}$$

or

$$Pe_h \frac{1}{(1 + \epsilon_H/\alpha)} \gg 1, \tag{51}$$

which for the laminar flow reads

$$Pe_h \gg 1. \tag{52}$$

In the turbulent regime, the inequality 51 determines the validity limit. ϵ_H is related to the friction factor through u_* leading to a dependency to Re. The left hand side of 51 is proportional to $Pr_h f(Re_h)$ where f increases with Re_h in a rate weaker than a linear function. Hence, still the solution is valid in high enough Peclet numbers, but the validity range is more sensitive to Pr than to Re.

Another restriction is deduced regarding the cold channel by considering the x-conduction to be trivial compared to the conduction in z_c-direction which leads to

$$L_0 \gg H_c,$$

or

$$Pe_h \frac{1}{(1 + \epsilon_H/\alpha)} \gg \frac{H_c}{H_h}. \tag{53}$$

Regarding the plate, since comparable temperature changes occur across L_0 and H_p, transversal heat conductions are negligible if

$$Pe_h \frac{1}{(1 + \epsilon_H/\alpha)} \gg \frac{H_p}{H_h} \tag{54}$$

which is automatically fulfilled if the requirement in the inequality 51 is met.

Considering the case $L < L_0$, we note that in an approximate manner $\Delta\theta_L$ decrease proportionally with L/L_0. Thus, as long as assumption 3 is met, the relations discussed in this section will still hold.

Similar relations can be written for the cold side parameters. In all, Pr and Re numbers in both channels need to be sufficiently large.

4.2. Calculation of heat transfer coefficient

The thermal performance of a PHE is directly linked to the heat flux through the plate, q_p which can be expressed based on the gradients of the temperature in z- direction. The temperature gradients appear as the first terms in Eq.s 5 & 6, according to which, the thermal performance is a function of Re, Pr as well as the length to height ratio (the diffusivity ratio is mainly a function of the Re and Pr numbers). If the length/ height is sufficiently great, the second terms (x and y gradients) vanish and the dependence of the local heat flux to the length-heigh ratio can be neglected.

We can derive a term to calculate q_p by using Eq.s 13 and 46,

$$q_p^* = -\sum_{m=1}^{\infty}\left[\left(\int_0^x -\Phi_x(x,y)e^{\lambda_m x}dx + (1-\Phi(0,y))\right)\rho_m e^{-\lambda_m x}\acute{\zeta}_m(-1)\right]. \tag{55}$$

As we aim to compare the results with external sources, we need to use dimentional heat flux,

$$Q_p = Aq_p = LW\frac{k_p}{H_p}(T_h^0 - T_c^0)\int_0^1\int_0^1 q_p^* dx\,dy. \tag{56}$$

The amount of the heat rejected from the hot side and the heat given to the cold side are also calculated as the following,

$$Q_h = C_h\left(T_h^0 - T_h^{out}\right), \tag{57a}$$

$$Q_c = C_c\left(T_c^{out} - T_c^0\right). \tag{57b}$$

In an ideal case where all heat transfer is carried out through the plate, the above-mentioned values are equal, i.e.

$$Q_p = Q_h = Q_c. \tag{58}$$

The rate of heat exchange is linked to the overall heat transfer coefficient, U as below [1, p. 29-33],

$$U = \frac{q_p}{F\,LMTD}, \tag{59a}$$

$$LMTD = \frac{\Delta T_1 - \Delta T_2}{log(\frac{\Delta T_1}{\Delta T_2})}, \tag{59b}$$

$$\Delta T_1 = T_h^0 - T_c^{out}, \quad \Delta T_2 = T_h^{out} - T_c^0. \tag{59c}$$

U is related to the convective heat transfer coefficients. Assuming no heat loss and no thermal resistance due to the fouling we can write

$$\frac{1}{U} = \frac{1}{h_h} + \frac{1}{h_c} + \frac{H_p}{K_p}. \tag{60}$$

For further calculations, by considering a similarity between the both channels, i.e. $h_h = h_c = h$, $k_h = k_c = k_{air}$ and $D_h = D_c = D$, the Nusselt number, $Nu = hD/k_{air}$ is obtained.

In the following, we evaluate the analytical solution by studying the thermal performance and temperature distribution for a heat exchanger section with smooth-surface plates, and we compare the results with external sources. In all cases, the channel dimensions and flow conditions in the hot and cold sides are considered to be similar, i.e. $L = W$, $H_h = H_c$, $Pr_h = Pr_c$ and $Re_h = Re_c$. In the laminar flow, $L/D = 30$ and in the turbulent cases, L/D is taken to be between 20 and 30 depending on the amount of Pr. The illustrated results in turbulence are all based on the power-law velocity profile as in Eq. 2c.

4.3. Nusselt number in laminar flow

Gut et. al. [25] suggested Nu correlations based on experiments for flat PHE with different configurations including symmetric or asymmetric pass-arrangements and cocurrent and countercurrent flows. However, their data were largely scattered within different configurations imposing uncertainty on their correlation. Other correlations are available for laminar internal flows with smooth wall surface. We use the empirical correlations for hydraulically developed and thermally developing flow between parallel plates one for constant temperature surfaces attributed to Stephen as reported in [26] and the other one for uniform heat flux from the surfaces attributed to Shah and London [20, p. 128] and [27, p. 5.63]. In cross-flow PHEs, the surface thermal condition does not match any of the above conditions. In a case with equal heat capacity flows in the channels, the surface temperature is almost constant around the line $y = x$ and the heat flux is almost fixed around the line $y = 1 - x$. The surface thermal condition is usually more important in smaller Pr values. Having noticed that, we use the available relations as estimations for the accuracy of the present analytical model.

Nu curves are illustrated in Fig. 2 for various values of Pr. As the benchmark curves are not valid for small Pr values, we limit the study to $Pr \geqslant 0.7$. The present model shows a close agreement with the empirical correlations, especially the case with constant temperature surface. Since the curves for the model and correlations follow similar slopes and hold almost uniform distances from each other,

it is understood that the functional forms of the curves are also in a good agreement. Although, the analytical results are consistency below the benchmarks, the differences are trivial and we are not able to attribute them to a specific source of error.

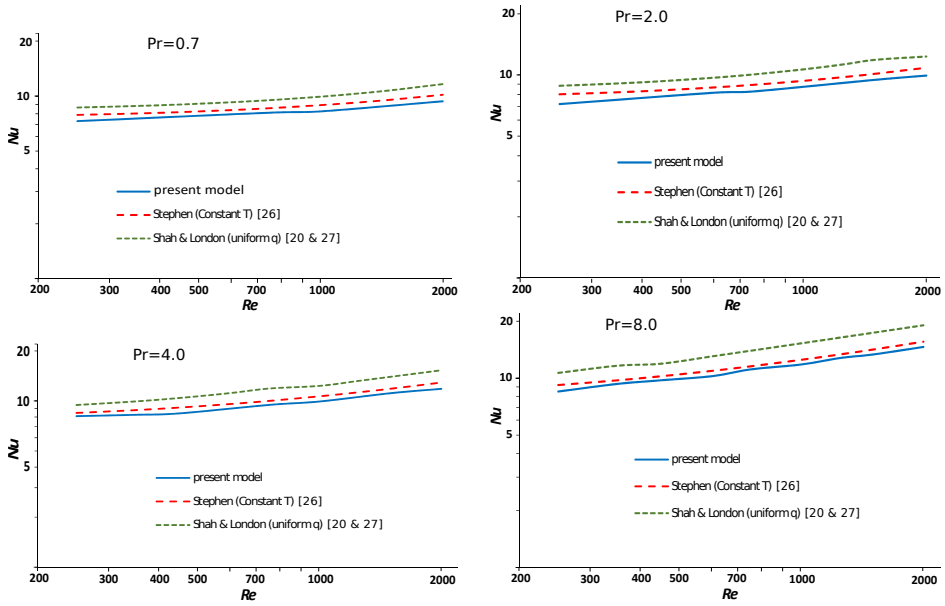

Figure 2: *Nu* profiles from the present model and empirical correlations for various *Pr* in the laminar regime.

4.4. Nusselt number in turbulent flow

Regarding the turbulent regime between parallel smooth plates, empirical correlations are available for small and large *Pr* numbers and we note that unlike the laminar regime, relations provided for circular pipes can also be used here as estimations. For an evaluation of the model, we use *Nu* expressions as described below.

The Ref.s [27, p. 5.23] [20, p. 379] provide correlations proposed by Notter and Sleicher, which are basically for flows into circular pipes and are valid for $0.04 \leqslant Pr \leqslant 0.1$, $10^4 \leqslant Re \leqslant 10^6$. The Taler's correlation [28] is based on a relationship for turbulent Prandtl number proposed by Aoki, and the validity range is declared to be $0.0001 \leqslant Pr \leqslant 0.1$, $3 \times 10^3 \leqslant Re \leqslant 10^6$. The Dwyer's relation as is represented in [29, p. 454] is for the flow of low *Pr* fluids between parallel plates with heat flux from the both plates. The correlation attributed to

Shibani and Ozisik [30] is for flows between parallel plates and is valid in $0.1 \leqslant Pr \leqslant 10^4$, $10^4 \leqslant Re \leqslant 10^6$. Finally, the original expression of Dittus-Boelter as is reported in [31, p. 544] is for flows in circular pipes and is valid in $0.7 \leqslant Pr \leqslant 120$, $2500 \leqslant Re \leqslant 1.24 \times 10^5$.

The present model is derived for a hydraulically developed but thermally developing flow. Since the above-mentioned correlations are represented for fully developed conditions, we use the relations proposed by Al-Arabi as is reported in Ref. [27, p. 5.27] to modify them for a thermally developing flow condition.

Fig. 3 depicts $Nu - Re$ curves in the range $0.05 \leqslant Pr \leqslant 4$. For each Pr, the empirical correlations are selected according to the declared range for their validity. In occasions we may have used the correlations beyond their declared validity range as approximations.

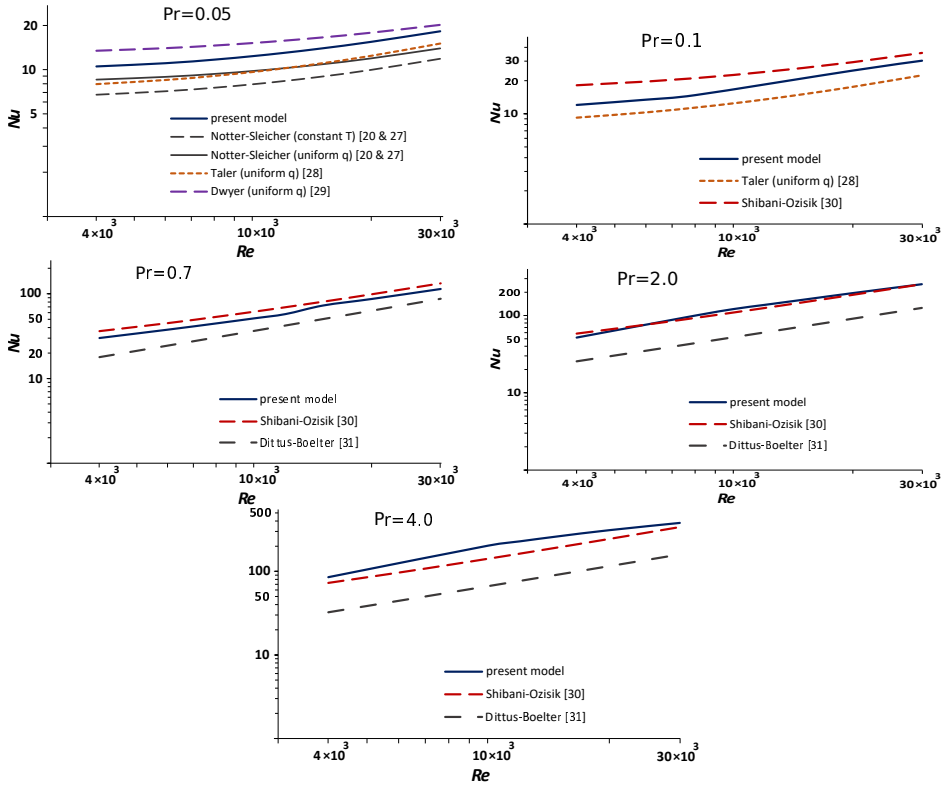

Figure 3: Nu profiles from the present model and empirical correlations for various Pr in turbulent regime.

We see in the figure that the present model is in a good agreement with the

other correlations in the displayed Pr and Re ranges, in terms of both the values and functional form with respect to Re. It should be noted that the relations such as Dittus-Boelter which are represented for circular pipes underestimate the heat transfer coefficients in the PHE geometry and are referred only as estimations. We also note that the accuracy of the empirical expressions themselves is limited and uncertainties around 25% are expected [31, p. 447]. Hence, in the displayed Pr and Re intervals, the uncertainties in the empirical correlations cover parts of the differences with the present model.

The present model tends to underestimate heat transfer coefficients in $Pr \leqslant 0.1$ especially when Re is not large i.e. $Pe < 1000$. In such conditions, the conductivity plays a major role in the heat transfer even in the core of the channel. Consequently, the temperature of the fluid in a channel will be highly affected by the temperature of the flow in the other side and hence, there will be a considerable temperature gradients along the stream direction resulting in transversal heat conductions in both x and y directions to be noteworthy heat transfer mechanisms. Since our model includes only the z-axis conduction and the other components are neglected, the predicted heat transfer coefficient will be smaller than reality. Eq. 5

For a better understanding about the effect of the transversal conduction, we have computed the amount of different heat transfer items as in Eq.s 56 and 57. According to the analytical solution, Q_p is smaller than Q_h and Q_c by up to 12% in $Pr = 0.05$ and 5% or less in $Pr \geqslant 0.5$ which indicates some heat leakage to/ from hot/ cold fluids on the side boundaries (walls), entrances and outlets. We will study this effect with more scrutiny later in the study of temperature distribution.

The selected profile for the eddy diffusivity in the channel cross-section has an influence on the results, especially in high Pe values. With the use of the profile in Eq. 3c, the first eigenvalues are usually small enough and the mathematical expressions are easily handled. However, more realistic profiles have been offered [22] which are expected to provide improved results.

Another cause of the differences can be attributed to the fact that the model lacks no-slip boundary conditions on the side walls (the peripheral walls) of the channels. This factor is expected to be noticeable only if the length and width are too small in which case, the convection in average will be stronger in comparison with a real case with limited channel length/ width. We discuss this topic later in the study of the temperature distribution.

We note that the power-law profile gives velocities larger than reality in the vicinity of the walls which results in greater heat transfer rates. However, regarding that the convection is not the main mechanism of heat transfer in the turbulent

sublayar, the approximation of the power-law profile is not expected to cause considerable errors in the results. We used a combined linear, power-law velocity profile according to 2d for a few cases which are not displayed here, and obtained results with limited improvements.

4.5. Temperature distribution

In this section, we study the temperature field obtained by the solution and compare it with the results from a numerical model. This represents a better understanding about the strengths and limitations of the present model and provides explanations about the sources of errors.

A sample case has been considered as the following, hot fluid: air at $1atm$ and $T_h^0 = 298\,K$, cold fluid: air at $1\,atm$ and $T_c^0 = 273\,K$, plate material: aluminium, $L = W = 0.300\,m$, $H_f = H_r = 0.010\,m$, $H_p = 0.001\,m$ and $Re_h = Re_c = 6000$.

The geometry, materials and boundary conditions at the inlets and mid-channels in the analytical and numerical models are the same. However, for the numerical model, we apply no-slip velocity and no-flux thermal boundary conditions on the side walls of the channels and the plate, whereas the analytical model does not take any boundary condition other than entrances and mid-channels.

The numerical results are computed by ANSYS-Fluent 19.2. A mesh with inflations normal to the plate is considered. A study has been carried out to verify mesh independence by comparing the results with cases having less number of layer elements and coarser meshes in x and y directions. For the final simulation, we have used a mesh with 15 layers in z- direction for each channel containing about $1.4M$ nodes and $2.5M$ elements in total which gives results without considerable differences to the coarser cases. We have used the standard $k-\epsilon$ as the turbulence model and found 300 iterations to be enough for the convergence.

Fig. 4 shows temperature contours on the plate. The analytical and numerical results are similar in general, but we can spot differences in two aspects; firstly, the range of temperature change in the analytical solution is larger than that of the numerical simulation, and secondly, as a result of applying no-flux boundary conditions on the walls, the contours in the numerical results are perpendicular to the boundaries. Both items are mainly associated with the assumptions leading to neglecting the diffusion terms in x and y directions.

First, we note that although the scale analysis shows that the conduction terms in x and y directions are negligible with respect to the z- direction, they are not forced to be zero. In fact, the values of heat flux on the plate surface i.e. q_x and q_y prescribed by the solution in Eq. 12 are non-zero for every location including the boundaries. If in reality, a different boundary condition is introduced on the

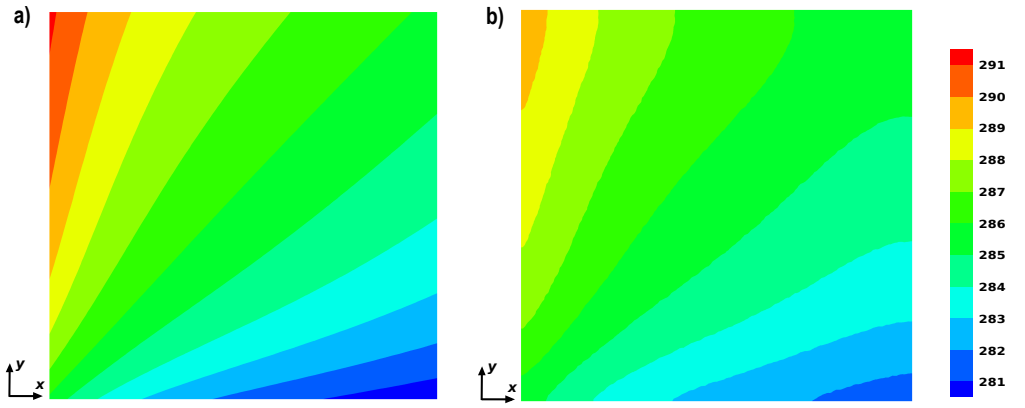

Figure 4: Temperature distribution (in Kelvin) on the plate surface from a) the analytical solution and b) the numerical model with no-heat flux on the walls.

walls, deviations will emerge from the results of the analytical solution. Here, compared to the numerical model with no heat-flux on the walls, extra heat inputs to the hotter boundaries and extra heat rejections from the colder boundaries are obtained from the analytical solution which explains why the range of temperature change in the analytical solution is larger than the numerical model.

Apart from the range, differences can also be seen in the pattern of the temperature field as the contours are perpendicular to the boundary in the numerical model which is associated with the no-flux boundary conditions. The deviations are rapidly decayed in the locations closer to an entrance while they are more spread in the areas with more distance from the entrances, because in farther distances from the entrances, the temperature field is nearly stabilized and heat flux in all directions are small and hence, the solution will be more sensitive to perturbations originated from the boundaries. However, these deviations are expected to cause an insignificant impact on the overall heat transfer as the rate of heat transfer is relatively small in the locations far from the entrances.

Fig. 5 depicts the temperature distribution on the $x-y$ plane at $z_h = 0.2$ in the hot channel. Compared to the results for the plate, the ranges of the temperature change are closer to each other and the main deviation is seen in the vicinity of the walls. A source of this deviation is the no-flux thermal boundary condition on the channel walls in the numerical model which is different from the analytical solution, but unlike the plate, due to the presence of the convection, the temperature gradients in the channels are relatively small and the results are less sensitive to the wall thermal boundary conditions. The deviation is to a large degree related to

the fact that in the numerical model, the no-slip boundary condition is applied on the walls whereas in the analytical solution as in assumption 3, the channels are regarded as infinitely wide. As a result, in the numerical model, the convection of the hot stream will be weaker in adjacent to the walls allowing the cold flow on the other side of the channel to have a greater influence on the temperature field through diffusion and hence, the temperatures near the walls are reduced. This results in the calculation of higher heat transfer rates in the analytical solution, especially if the length of the channel is small.

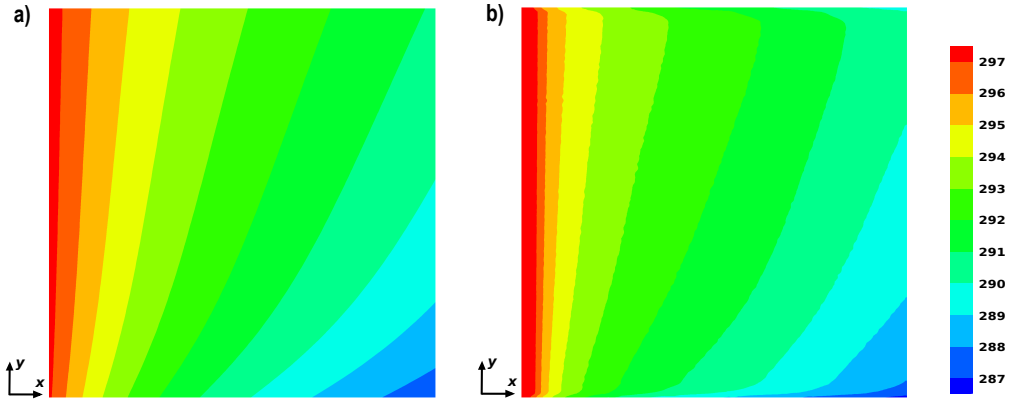

Figure 5: Temperature distribution (in Kelvin) on the plane $z_h = 0.2$ from a) the analytical solution and b) the numerical model with no-heat flux on the walls.

The temperature curves across the channel depth for a few (x, y) points are displayed in Fig. 6. The slope of the curves is higher in the locations where the convection is weaker or in the areas close to an entrance. The maximum gradient at each point occurs at the plate surface and reflects the local rate of heat transfer between the channels.

Fig. 6 shows that the curve for point 1 has wavering forms in both channels, i.e. the temperature falls slightly below the cold-side entrance value in the cold channel and goes slightly beyond the hot-side entrance in the hot channel. A similar pattern is seen for point 2 only in the hot channel. The reason for these wavering forms which may occur only in the vicinity of the entrances is related to the fact that the sequence ρ_m in the solution (Eq. 35 for the hot side) is oscillating. As the terms $e^{-\lambda_m x}$ decay in moderate and large x values, the wavering form is seen only in the areas close to an entrance. We note that the terms $e^{-\lambda_m x}$ will also diminish if the eigenvalue λ_m is large. Therefore, it is important that the largest eigenvalue of the solution must be great enough to minimize errors related

to neglecting the remaining terms and provide sufficient accuracies, especially in locations close to the entrances.

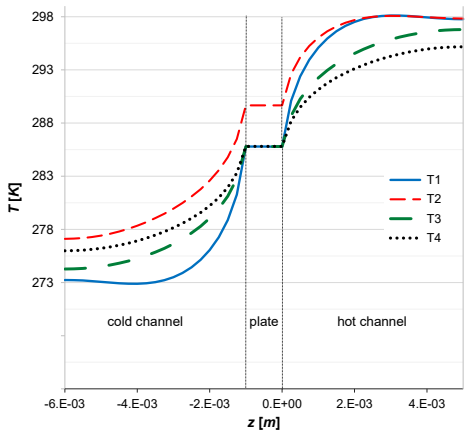

Figure 6: $T(z)$ curves from the analytical solution showing temperature variations along lines in z direction at selected x, y points. The indexes for the temperatures correspond to the locations as follow; $(x_1, y_1) = (0.1, 0.1)$, $(x_2, y_2) = (0.1, 0.9)$, $(x_3, y_3) = (0.5, 0.5)$ and $(x_4, y_4) = (0.9, 0.9)$.

Conclusions

In the present study, an analytical solution is developed for heat transfer in a cross-flow PHE, providing the temperature field in the plate and channels. The solution takes into account the major conduction-convection mechanisms in 3-dimensions for both laminar and turbulent flows which to the best of our knowledge, is the most comprehensive model for such physics.

The results of the model are compared with empirical correlations for Nu number. In the laminar regime, the model shows a close agreement with experiment for a wide range of Pr and Re numbers. A close agreement is also seen in turbulence for $Pe > 10000$ (and for smaller Pe numbers if Pr is not too small), as in small Pe numbers, transversal heat conduction (including axial conduction) limits the accuracy of the model. There is also a restriction in high Pe values which is thought to be due to sensitivity to the profile of the turbulent eddy diffusivity and can be amended by using a more accurate profile. An additional study regarding the temperature distribution with air as the fluid in a turbulent regime demonstrates that transversal heat conduction is partly linked to the boundary conditions on the side walls.

The obtained solution is in the form of infinite series and needs to be truncated at some point which poses an error to the solution and may also lead to a wavering pattern for the temperature in locations close to the channel entrances.

The present study offers a tool for better understanding of heat transfer in the cross-flow heat exchangers with flat-surface plates. The model in its present form can be used for rough surfaces by choosing appropriate friction factor for the calculation of the turbulent eddy viscosity. However, due to the flexibility of the model in the selection of different parameters for the eddy viscosity and the velocity profile, we expect that it can be adjusted for applications with surfaces having macroscopic irregularities provided that irregularities are uniformly distributed and are small compared to the boundary layer (channel height) and an effective surface can be defined. Also, in MEEs with flat membranes, as long as the impact of the mass transfer on the energy balance is negligible, we expect that the present model can be used directly or by modifications, to give predictions about their thermal performance. In a more general sense, the methodology employed to solve the problem may be useful for analysis of other problems with separated flows and coupled boundary conditions.

Appendixes

A. *Solution of the differential equation for Z in the channel*

Eq. 20 can be rearranged for each eigenvalue λ_m as

$$\left(1+\frac{\epsilon_H(z_h)}{\alpha}\right)\frac{\partial^2 Z(z_h)}{\partial z_h^2}+\frac{1}{\alpha}\frac{\partial \epsilon_H(z_h)}{\partial z_h}\frac{\partial Z(z_h)}{\partial z_h}+Pe\, f_u(z_h)\frac{H_h}{8L}\lambda_m Z(z_h)=0. \qquad (A.1)$$

Since $\left(1+\frac{\epsilon_H(z_h)}{\alpha}\right)\neq 0$ and the other coefficients are bounded, we can consider the solution as $Z(z_h)=\sum_0^\infty a_i z_h^i$ for $-1\leqslant z_h\leqslant 0$. A polynomial expression can be derived for $f_u(z_h)$ from Eq. 2 using the Maclaurin series. The new expression for $f_u(z_h)$ together with Eq. 3 for $\epsilon_H(z_h)$ and the series expression for $Z(z_h)$ are substituted into Eq. A.1. In the resulting equation, we can consider the coefficients for each power of z_h to be zero. Consequently, for a desired N_a, we will find a_i, $i=2,3,4,....,N_a$ in terms of a_0 and a_1 which are independent coefficients and correspond to $\zeta(z_h)$ and $\xi(z_h)$ respectively. The first terms of ζ_m with $a_0=1$ and

$a_1 = 0$ are as follows

$$a_2 = -\frac{d\lambda_m}{2}, \tag{A.2a}$$

$$a_3 = -\frac{d\lambda_m}{6n}, \tag{A.2b}$$

$$a_4 = \frac{d\lambda_m}{24}\left(d\lambda_m + \frac{6\frac{\epsilon_0}{\alpha}}{1+\frac{\epsilon_0}{\alpha}} + \frac{n-1}{n^2}\right). \tag{A.2c}$$

where $d = \frac{H_h}{L}\frac{Pe}{(1+\epsilon_0/\alpha)}$ is a measure of the ratio between the rate of streamwise convection and the strength of the conduction perpendicular to the plate.

B. Deriving $\Phi(x, y)$ from the continuity of heat flux

We can derive expressions for $\Phi_c(x, y)$, $\Phi_{c,y}(x, y)$ and $\Phi_c(x, 0)$ from Eq. 46 and substitute them into Eq. 44 to obtain

$$\begin{aligned}\sum_{m=1}^{\infty}\left[\left(\int_0^x \Phi_x(x,y)e^{\lambda_m x}dx-(1-\Phi(0,y))\right)\rho_m e^{-\lambda_m x}\acute{\zeta}_m(-1)\right] = \\ \sum_{n=1}^{\infty}\left[\left(\int_0^y \left\{\Phi_y(x,y)+\sum_{i=1}^{\infty}\left[\left(\int_0^x -\Phi_{xy}(x,y)e^{\lambda_i x}dx-\Phi_y(0,y)\right)\rho_i e^{-\lambda_i x}\acute{\zeta}_i(-1)\right]\right\}e^{\lambda_n y}dy \right.\right. \\ \left.\left. -\frac{1}{1+\sum_{j=1}^{\infty}\left(\rho_{c,j}\acute{\zeta}_{c,j}(-1)\right)}\Phi(x,0)\right)\rho_{c,n}e^{-\lambda_n y}\acute{\zeta}_{c,n}(-1)\right],\end{aligned} \tag{B.1}$$

which is a partial integro-differential equation for $\Phi(x, y)$. We consider a two-variable power series as the ansatz expression for $\Phi(x, y)$, i.e.

$$\Phi(x,y) = \sum_{i=0}^{\infty}\sum_{j=0}^{\infty} b_{ij}x^i y^j, \tag{B.2}$$

which together with its x and y derivatives can be substituted into Eq. B.1. We can then consider the coefficients of the $x^i y^j$ terms to sum up to zero. Despite its complex appearance, the obtained system of equations is analytically solvable for a desired number of terms, N_b, and provides explicit and interpretable expressions for b_{ij}, $i, j = 0, 1, 2, ..., N_b$. For example, the first coefficient which is the temperature at $(x, y) = (0, 0)$ and represents an estimation for the average temperature of the plate is as below,

$$b_{00} = \frac{g_h}{g_h + g_c}. \tag{B.3}$$

where $g_h = \sum_{m=1}^{N_b} \rho_m \acute{\zeta}_m(-1)$ and $g_c = \sum_{n=1}^{N_b} \rho_{c,n} \acute{\zeta}_{c,n}(-1)$ are representatives for the thermal strength of the hot and cold channels respectively.

References

[1] T. Kuppan. *Heat Exchanger Design Handbook*. Marcel Dekker, 2000.

[2] J. A. W. Gut and J. M. Pinto. Modeling of plate heat exchangers with generalized configurations. *Int. J. Heat Mass Tran.*, 46:2571–2585, 2003.

[3] W. Y. Saman and S. Alizadeh. Modelling and performance analysis of a cross-flow type plate heat exchanger for dehumidification / cooling. *Sol. Energy*, 70(4):361–372, 2001.

[4] L. Z. Zhang. Heat and mass transfer in a cross-flow membrane-based enthalpy exchanger under naturally formed boundary conditions. *Int. J. Heat Mass Tran.*, 50:151–162, 2007.

[5] S. M. Huang, L. Z. Zhang, K. Tang, and L. X. Pei. Fluid flow and heat mass transfer in membrane parallel-plates channels used for liquid desiccant air dehumidification. *Int. J. Heat Mass Tran.*, 55:2571–2580, 2012.

[6] M. Simonetti, G. V. Fracastoro, G. Chiesa, and S. Sola. Numerical optimization and experimental testing of a new low pressure heat exchanger (LoPHEx) for passive ventilation of buildings. *Appl. Therm. Eng.*, 103:720–729, 2016.

[7] A. Vali, G. Ge, R. W. Besant, and C. J. Simonson. Numerical modeling of fluid flow and coupled heat and mass transfer in a counter-cross-flow parallel-plate liquid-to-air membrane energy exchanger. *Int. J. Heat Mass Tran.*, 89:1258–1276, 2015.

[8] S. Jun and V. M. Puri. A 2d dynamic model for fouling performance of plate heat exchangers. *J. Food Eng.*, 75:364–374, 2006.

[9] F. C. C. Galeazzo, R. Y. Miura, J. A. W. Gut, and C. C. Tadini. Experimental and numerical heat transfer in a plate heat exchanger. *Chem. Eng. Sc.*, 61, 2006.

[10] V. I. Deshko, A. Y. Karvatskii, and I. O. Sukhodub. Heat and mass transfer in cross-flow air-to-air membrane heat exchanger in heating mode. *Appl. Therm. Eng.*, 100:133–145, 2016.

[11] V. Dvořák and T. Vít. CAE methods for plate heat exchanger design. *Energy Proced.*, 134:234–243, 2017.

[12] T. Zaleski and K. Klepacka. Approximate method of solving equations for plate heat exchangers. *Int. J. Heat Mass Tran.*, 35(5):1125–1130, 1992.

[13] N. Srihari, B. P. Rao, B. Sunden, and S. K. Das. Transient response of plate heat exchangers considering effect of flow maldistribution. *Int. J. Heat Mass Tran.*, 48:3231–3243, 2005.

[14] L. Z. Zhang and J. L. Niu. Effectiveness correlations for heat and moisture transfer processes in an enthalpy exchanger with membrane cores. *T. ASAE*, 124:922–929, 2002.

[15] A. R. A. Khaled. Analysis of heat transfers inside counterflow plate heat exchanger augmented by an auxiliary fluid flow. *Sci. World J.*, 2014:308545, 2014.

[16] H. M. Yeh and C. D. Ho. Numerical analysis on heat transfer in parallel-flow rectangular recuperators with internal recycle. *J. Appl. Sci. Eng.*, 15(1): 59–68, 2012.

[17] W. Lu, T. Zhang, M. Yang, and Y. Wu. Analytical solutions of force convective heat transfer in plate heat exchangers partially filled with metal foams. *Int. J. Heat Mass Tran.*, 110:476–481, 2017.

[18] R. Sangsawang, T. Matum, and U. Nontakaew. Analytical solution for the temperature distribution in cross-flow plate heat exchanger channels of isosceles triangular geometry. *Mech. Eng. Int. J.*, 1(2):1–10, 2014.

[19] B. R. Munson, T. H. Okiishi, W. W. Huebsch, and A. P. Rothmayer. *Fundamentals of fluid mechanics*. John Wiley & Sons, 7th edition, 2013.

[20] A. Bejan. *Convection heat transfer*. John Wiley & Sons, 4th edition, 2013.

[21] M. R. Malik. *Prediction of laminar and turbulent flow heat transfer in annular passages*. PhD thesis, Iowa State University, 1978.

[22] J. Guo. Eddy viscosity and complete log-law for turbulent pipe flow at high Reynolds numbers. *J. Hydraul. Res.*, 1686:1–13, 2016.

[23] H. Schlichting. *Boundary-layer theory*. McGraw-Hill, 1979.

[24] R. Haberman. *Applied partial differential equations with Fourier series and boundary value problems*. Pearson, 4th edition, 2004.

[25] J. A. W. Gut, R. Fernandes, J. M. Pinto, and C. C. Tadini. Thermal model validation of plate heat exchangers with generalized configurations. *Chem. Eng. Sc.*, 59:4591–4600, 2004.

[26] Y. S. Muzychka and M. M. Yovanovich. Laminar forced convection heat transfer in the combined entry region of non-circular ducts. *J. Heat Trans*, 126(1):54–61, 2004.

[27] M. A. Ebadian and Z. F. Dong. Forced convection, internal flow in ducts. In W. M. Rohsenow, J. R. Hartnett, and Y. I. Cho, editors, *Handbook of Heat Transfer*, chapter 5. McGraw-Hill, 3rd edition, 1998.

[28] D. Taler. Heat transfer in turbulent tube flow of liquid metals. *Procedia Eng.*, 157:148–157, 2016.

[29] Robert Stieglitz. Low prandtl number thermal-hydraulics. In Concetta Fazio, editor, *Handbook on Lead-bismuth Eutectic Alloy and Lead Properties, Materials Compatibility, Thermal-hydraulics and Technologies*, chapter 10. OECD, 2007.

[30] F. D. Haynes and G.D. Ashton. Turbulent heat transfer in large aspect channels. Technical Report CRREL Report 79-13, U.S. Army Cold Regions Research and Engineering Laboratory, 1979.

[31] T. l. Bergman, A. S. Lavine, F. P. Incropera, and D. P. Dewitt. *Fundamentals of Heat and Mass Transfer*. John Wiley & Sons, 2011.